Vibrationally Mediated Photodissociation of $C_2H_4^+$†

Myung Hwa Kim,‡,§,‖ Brian D. Leskiw,‡,⊥ Lei Shen,‡ and Arthur G. Suits*,‡,§

Department of Chemistry, Wayne State University, Detroit, Michigan 48202, and Department of Chemistry, State University of New York Stony Brook, Stony Brook, New York 11794-3400

Received: February 16, 2007; In Final Form: May 3, 2007

We report the vibrationally mediated photodissociation dynamics of $C_2H_4^+$ excited through the $\tilde{B}^2A_g$ state. Vibrational state-selected ions were prepared by two-photon resonant, three-photon ionization of ethylene via (π, 3s) and (π, 3p) Rydberg intermediate states in the wavelength range 298−349 nm. Absorption of a fourth photon led to dissociation of the cation, and images of the product ions $C_2H_3^+$ and $C_2H_2^+$ were simultaneously recorded using reflectron multimass velocity map imaging. Analysis of the multimass images yielded, with high precision, both the total translational energy distributions for the two dissociation channels and the branching between them as a function of excitation energy. The dissociation of ions that were initially prepared with torsional excitation exceeding the barrier to planarity in the cation ground state consistently gave enhanced branching to the H elimination channel. The results are discussed in terms of the influence of the initial state preparation on the competition between the internal conversion to the ground state and to the first excited state.

I. Introduction

The vibrationally mediated photodissociation technique pioneered by Crim and co-workers[1−3] has been very successful in revealing the features of the ground- and the excited-state potential surfaces of molecules and, in some cases, achieving laser control of the outcome of uni- and bimolecular reactions. The experimental method relies upon photodissociation from well-characterized initial vibrational states of neutral molecules, with Franck−Condon factors then determining the access to distinct regions of the excited-state surfaces.[1] State-prepared ion photodissociation and ion−molecule reaction dynamic studies have also been used to explore more related phenomena in ionic systems. Anderson and co-workers have investigated the reaction of the mode-selective vibrational excitation of polyatomic cations with neutral molecules using a resonance-enhanced multiphoton ionization (REMPI) process for state preparation.[4−6] Very recently, velocity map ion imaging[7,8] and slice imaging techniques[9−11] combined with REMPI have successfully been applied to exploring, in detail, the photodissociation dynamics of the state-selected molecular ions such as Br_2^+,[12] CF_3I^+,[13] $BrCl^+$,[14] DCl^+, [15] OCS^+,[16] and $CH_3CH_2CHO^+$.[17,18] In these experiments, a parent ion is initially created in a single and well-defined electronic, spin−orbit, and vibrational state by REMPI, and then the ion is dissociated into fragments by a second photolysis laser or by another photon from the same laser.[14] The main advantage of these techniques is that the resulting images allow for the direct extraction of the velocity and of the angular distribution of the fragments, which provides insight into the photofragmentation dynamics of molecular ions.

Unimolecular decomposition of $C_2H_4^+$ has been extensively investigated as a prototype system in the study of both the electronic relaxation mechanisms and the influence of conical intersections on dissociation dynamics, both experimentally[19−22] and theoretically.[23−26] It has been well-established that an electronically excited $C_2H_4^+$ ion undergoes unimolecular decomposition via H and H_2 elimination. From previous threshold photoelectron−photoion coincidence (TPEPICO) and photoionization mass spectrometry (PIMS) experiments and theoretical studies, the thresholds for the elimination of H and H_2 from $C_2H_4^+$ are found to exhibit different correlations to the electronic states involved in the dissociation, and they are very close in energy:

$$C_2H_4^+(\tilde{X}^2B_{3u}) + h\nu \rightarrow C_2H_3^+ + H \quad 2.70\ (\pm 0.01)\ \text{eV} \qquad (1)$$

$$\rightarrow C_2H_2^+ + H_2 \quad 2.62\ (\pm 0.02)\ \text{eV} \qquad (2)$$

On the basis of the good agreement with the predicted branching between these two channels using quasiequilibrium theory (QET), Stockbauer and Inghram[19] suggested that the two comparative dissociation pathways closely follow a statistical decay pattern. On the other hand, Lorquet and co-workers[23,24] have found theoretical evidence supporting the view that the dissociation of $C_2H_4^+$ involves several electronic exited states above the cation electronic ground state. They concluded that the nonadiabatic coupling between the cationic electronic ground state ($\tilde{X}^2B_{3u}$) and the first electronically excited state ($\tilde{A}^2B_{3g}$) via a conical intersection is involved in one of the dissociation pathways, depending on the initial excited electronic state. For the dissociation from the $\tilde{B}^2A_g$ excited state, however, they also suggested that the $C_2H_2^+$ channel can proceed adiabatically by the transformation into an isomerized ethylidene (CH_3CH^+) structure in its electronic ground state, $\tilde{X}^2B_{3u}$. The $C_2H_3^+$ channel, however, requires electronic coupling to the $\tilde{A}^2B_{3g}$ state through excitation of the torsional vibration (ν_4) around the

† Part of the "Roger E. Miller Memorial Issue"

* E-mail: asuits@chem.wayne.edu.
‡ Wayne State University.
§ State University of New York Stony Brook.
‖ Present address: Department of Chemistry & Bichemistry, University of California at Santa Barbara, Santa Barbara, CA, 93106.
⊥ Present address: Department of Chemistry, Youngstown State University, Youngstown, OH, 44555.

10.1021/jp071348k CCC: $37.00
Published on Web 07/10/2007

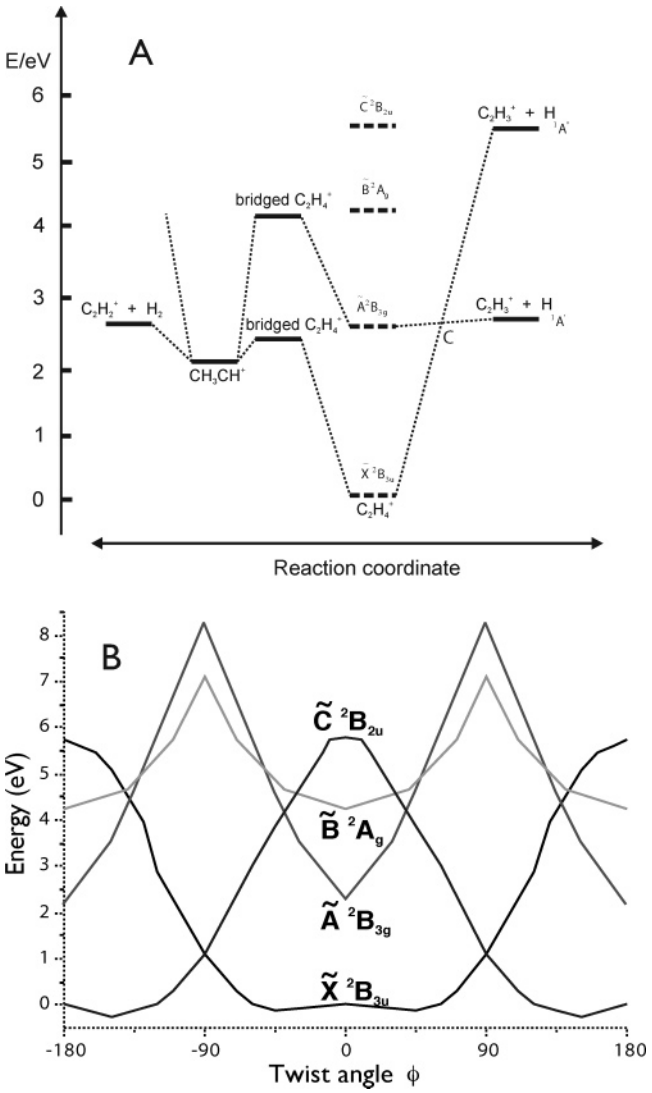

Figure 1. Schematic diagrams for potential energy surfaces of $C_2H_4^+$. Adapted from ref. 23. Note that the point of C is the conical intersection between the $\tilde{X}^2B_{3u}$ and the $\tilde{A}^2B_{3g}$ state along the C−H stretching mode.

conical intersection along the C−H stretching coordinate (ν_1), which correlates asymptotically to the lowest dissociation pathway, $C_2H_3^+ + H$, as shown in the potential energy surface of Figure 1. Furthermore, previous experimental and theoretical results suggest that there is no evidence of exit channel barriers for H atom or H_2 molecule ejection from the ethylene cation. The competition between these pathways can provide insight into the complex coupling among the accessible cation electronic states.

We recently developed a versatile reflectron velocity map imaging apparatus that can be employed in a multimass configuration[27] to simultaneously obtain the full velocity distributions and the branching fractions for multiple masses.[28,29] We demonstrated the capability of this technique in the state-selected photodissociation of $C_2H_4^+$ ions through vibronic bands of (π, nf) Rydberg states in the vicinity of the ionization potential of ethylene,[30] and we recently extended the technique to document conformationally controlled dissociation as well.[18] In the multimass ethylene cation studies, we simultaneously recorded images of photofragment $C_2H_3^+$ and $C_2H_2^+$ ions and directly obtained the velocity distribution and the branching fraction ratios for these competitive dissociation pathways.

The present paper focuses on photodissociation dynamics of $C_2H_4^+$ through a broad range of levels of the $\tilde{B}^2A_g$ excited state. The cation is prepared in a range of vibrational levels of the ground electronic state by two-photon resonant and three-photon ionization via (π, 3s) and (π, 3p) Rydberg intermediate states. Photoelectron imaging, combined with REMPI, is used to confirm the nature of the vibronic transitions that give rise to the initial vibrational state selections of the ground electronic state of ions, while providing additional detail into the photoionization dynamics.

II. Experimental Procedures

The reflectron multimass velocity map ion imaging apparatus used in this study is described in more detail elsewhere,[30] and only a brief sketch is given here. The apparatus consists of a source chamber, a reaction chamber with ion optics and two orthogonal sets of deflection plates, a single stage reflectron, and a microchannelplate (MCP)/phosphor detector. A pulsed supersonic molecular beam of ethylene (Linde, CP Grade, 99.5%) is made by expanding ethylene molecules, which are diluted to about 5% with helium at a backing pressure of 1.2 bar, from a piezoelectric pulsed nozzle into the source chamber of our differentially pumped apparatus. After passing through a 1 mm diameter skimmer located 3.8 cm downstream of the pulsed nozzle orifice and then through a 2 mm collimator, the supersonic molecular beam enters into a velocity mapping ion optics assembly consisting of four electrodes. The molecular beam is perpendicularly intersected with a laser beam tuned to a two-photon resonant excitation of Rydberg states of ethylene. The operating pressures were maintained at $\sim 1.0 \times 10^{-5}$ Torr in the source chamber and at $\leq 5.0 \times 10^{-8}$ Torr in the main chamber. The laser light in the present study was generated by frequency doubling of the output of dye lasers pumped by the second harmonic (532 nm) of a neodymium:yttrium:aluminum garnet laser. The laser beam was vertically polarized, parallel to the detector surface, and then was focused with a lens ($f =$ 20 cm) into the interaction volume to cross the pulsed molecular beam. Typical output power for the pulsed dye laser beam entering the chamber was 0.3−0.5 mJ/pulse. The laser output spanned a wavelength range from 298 to 349 nm. Wavelength calibration was achieved using a wavemeter (Coherent WaveMaster). In these experiments, a single laser was used to ionize the C_2H_4 and to photodissociate the resulting $C_2H_4^+$ ions. It should be noted that, even though we did not record the REMPI spectrum of ethylene via the (π, 3s) and (π, 3p) Rydberg state, we carefully tuned the wavelengths on the basis of two previously reported REMPI spectra of ethylene.[31,32] We found excellent agreement with the previously reported transition energies and vibrational assignments. Both ionization and dissociation occur within the same laser pulse. After ionization occurred, the photofragments were accelerated through the multilens velocity mapping assembly, up to a kinetic energy of 4 kV. After passing through a field free region, the ion packets entered into a region with two plates of opposite polarity that were located 635 mm downstream from the interaction volume. The plates were then pulsed to ±225 V for 150 ns to separate the ions of different masses spatially according to their mass-to-charge ratio. After the ions were spatially dispersed, they entered a single stage reflectron consisting of the stack of 36 electrodes. In this region, the ions turn around due to the retarding field of the reflectron and are reaccelerated toward a detector through another field free region. The ions of different masses finally impact upon a position sensitive dual MCP/P-47 phosphor screen of 120 mm diameter (Burle). A 1.2 μs high-voltage pulse was applied to the MCP for the time gate of the $C_2H_4^+$, $C_2H_3^+$, and $C_2H_2^+$ ions, and the resulting images were

recorded using a CCD camera (Sony XT-ST50, 768 × 494 pixels) in conjunction with the IMACQ megapixel acquisition software[33] developed by our group, which permitted real-time event-counting and centroiding of the data. The signals were typically accumulated for 10 000 laser shots for each data set. The calibration of our images was achieved on the basis of the experimentally observed images of CO ($v = 0$, $J = 65$) in the photodissociation of OCS at 230 nm, while all apparatus parameters were kept the same.

Photoelectron images were obtained using the same instrument, although modified with a shorter linear flight path (~90 cm) and with reversed potentials, to confirm the ionic state distributions prepared by the (2 + 1) REMPI process. In this configuration, the main chamber and the flight path were shielded with a μ-metal sheet to avoid the influence of external magnetic fields. For (π, 3s) Rydberg states, the photoelectron background signal in this work was negligible, so that no background correction was required. However, for (π, 3p) Rydberg states, all images showed some background signal around the center of the images. This likely originated from photoelectrons produced by scattered light from the ion optics electrodes. Background images, which were collected by turning off the molecular beam, were thus subtracted from actual images under the same experimental conditions. Three-dimensional (3D) velocity distributions were then reconstructed from the projected images using the basis set expansion (BASEX) method developed by Reisler and co-workers.[34] To obtain the photoelectron kinetic energy distributions, the observed electron images for (π, 3s) Rydberg states were calibrated with a photoelectron image of ethylene (ionization potential (IP) = 10.5127 eV) at 58 160 cm^{-1}, which was one of the (2 + 1) REMPI transitions that has been well characterized in previous photoelectron spectroscopy studies.[35−37] The observed electron images for the (π, 3p) Rydberg states were calibrated with a photoelectron image of N_2O (IP = 12.8898 eV) on the origin ($3p\sigma^1\Pi$) of the (3 + 1) REMPI transition at 83 200 cm^{-1} due to the much higher electron kinetic energy as compared to the (π, 3s) Rydberg states.[38,39]

III. Results and Discussion

Photoelectron Images via 3s and 3p Rydberg States. The (2 + 1) REMPI photoelectron images obtained from single-color, two-photon resonant and three-photon ionization of C_2H_4 via the various 3s Rydberg states are shown in Figure 2. According to the previous REMPI studies,[31,32] the two-photon transition from the electronic ground state to the 1^1B_{3u} (π, 3s) Rydberg state is electronically forbidden, but it can be vibronically allowed through torsional excitation (υ_4), which leads to a dominant activity of υ_4 in the excitation spectrum. All images obtained through excitation at odd quanta pure torsional modes or through combination modes involving the C−C stretching (υ_2) clearly show a single sharp structure with very weak rings. The photoelectron spectra obtained from the reconstructed images also show the same strong features with very weak side peaks. In the case of the photoelectron spectrum taken at 58 160 cm^{-1}, which is the most intense and sharp resonance in the REMPI spectrum, the predominant peak corresponds to ions with 764.6 cm^{-1} of internal energy and is assigned as three quanta of υ_4^+ excitation, which is consistent with Franck−Condon diagonal ionization from a Rydberg state with a very similar geometry to that of the ground-state ion. The very weak side bands correspond to ionization through non-diagonal transitions to the 1, 5, and 6 anharmonic levels of the υ_4^+ mode in the ionic ground state, which indicates small changes in the C−C twisting angle upon ionization. Similarly, with the observed electron kinetic energies and the known photon energy, we assigned the predominant peaks in other transitions as those originating from the diagonal transitions ($\Delta v = 0$) of the same levels of the Rydberg states, consistent with a previous conventional magnetic bottle REMPI photoelectron spectroscopy (PES) result.[32] Our results illustrate that it is possible to prepare $C_2H_4^+$ ions with narrow, sometimes pure, vibrational state distributions, with each state corresponding to different types of motion.

As shown in Figure 3, the photoelectron images taken with (2 + 1) REMPI via (π, 3p) Rydberg states show sharp features at higher energy with broad structures at lower energy. In all cases, similar to the (π, 3s) Rydberg state, our resolution for electron kinetic energy cannot resolve these sharp structures, yet the diagonal transition is clearly dominant and consistent with previous results. An additional interesting feature of these photoelectron spectra is that we observe lower electron kinetic energy peaks that were absent in previous REMPI-PES[32] spectra at the same excitation energy. For the REMPI-PES spectrum of the $3p_z\ 0^0$ transition at $2\tilde{\nu} = 63\ 236\ cm^{-1}$, displayed in Figure 3, we see that an internal vibrational energy of 0.73 eV (5807 cm^{-1}) at the peak around 0.509 eV is closely matched with the energy separation of the 57 338 and 63 236 cm^{-1} energy values for the origin of the (π, 3s) Rydberg state and (π, $3p_z$) Rydberg state, respectively. This behavior is systematically observed in all photoelectron spectra obtained via the (π, 3p) Rydberg states in our study. These observations can be attributed to the coupling within the Rydberg manifold, for example, Rydberg−Rydberg coupling between the (π, 3s) and the (π, 3p) Rydberg states. It is apparent that if any of the three (π, 3p) Rydberg states were vibronically coupled to the (π, 3s) Rydberg state, then the photoelectron spectra taken via the (π, 3p) Rydberg states would also contain evidence of ionization from highly vibrationally excited levels of the (π, 3s) Rydberg state, as Rijkenberg and Buma mentioned from their REMPI-PES study of ethylene.[32] Our present photoelectron spectra show slow electron peaks in close proximity to these estimated electron kinetic energy values, which suggests that vibronic coupling between the Rydberg states is indeed involved during the (2 + 1) REMPI of ethylene. For the 2^1A_{3g} (π, $3p_x$) Rydberg states, in particular, we observe the coupling between the (π, $3p_x$) and the (π, $3p_y$) and (π, $3p_z$) Rydberg states as well as between the (π, $3p_x$) and the (π, 3s) Rydberg states, as shown in Figure 3. This kind of behavior, that is, the appearance of the various slow electron peaks in REMPI-PES spectra that closely match with various Rydberg origins at lower excitation energies, has previously been reported for the jet-cooled REMPI-PES experiments with sulfur containing molecules (CH_2SCH_2,[40] CH_3SH,[41] and CH_3SOCH_3[42]), methyl iodide,[43] and pyrazine.[44] This phenomenon was interpreted in terms of the inter-Rydberg state vibronic mixing between the two-photon resonant origin of Rydberg state and the accidental near-resonant excited vibrational levels of various lower lying Rydberg states.[45] As mentioned above, our results are in clear contrast to the REMPI-PES study by Rijkenberg and Buma on the same system.[32] The behavior was likely not observed in their data due to poor collection efficiency for photoelectrons with low kinetic energy.

Multimass Images from Vibrationally Mediated Photodissociation. The multimass velocity map images for photodissociation of state-selected $C_2H_4^+$, produced by 2 + 1 REMPI via the various vibronic bands of (π, 3s) and (π, 3p) Rydberg state, are presented in Figure 4. In all images, the linearly polarized laser light is vertical in the plane of the figure. It is

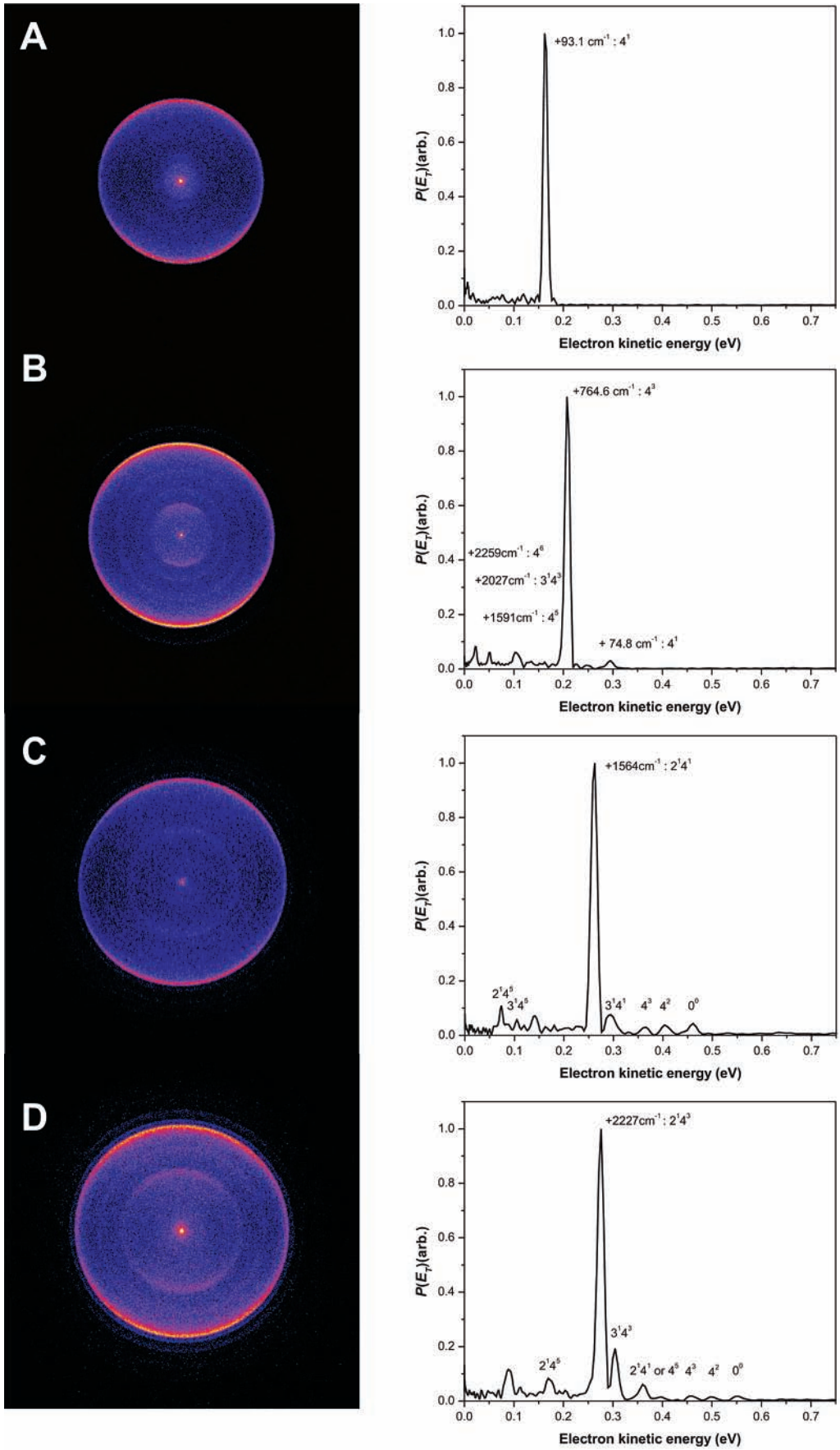

Figure 2. Photoelectron images and kinetic energy distributions measured by two-photon resonant, three-photon ionization via (π, 3s) Rydberg states at two-photon resonance energy of (A) 57 460 cm^{-1}, one quanta excitation of torsional mode (υ_4); (B) 58 160 cm^{-1}, three quanta excitation of torsional mode (υ_4); (C) 58 985 cm^{-1}, combinational excitation of one quanta of torsional (υ_4) and one quanta of C−C stretching modes (υ_2); and (D) 59 514 cm^{-1}, combinational excitation of one quanta of torsional (υ_4) and one quanta of CH_2 scissors modes (υ_3), respectively.

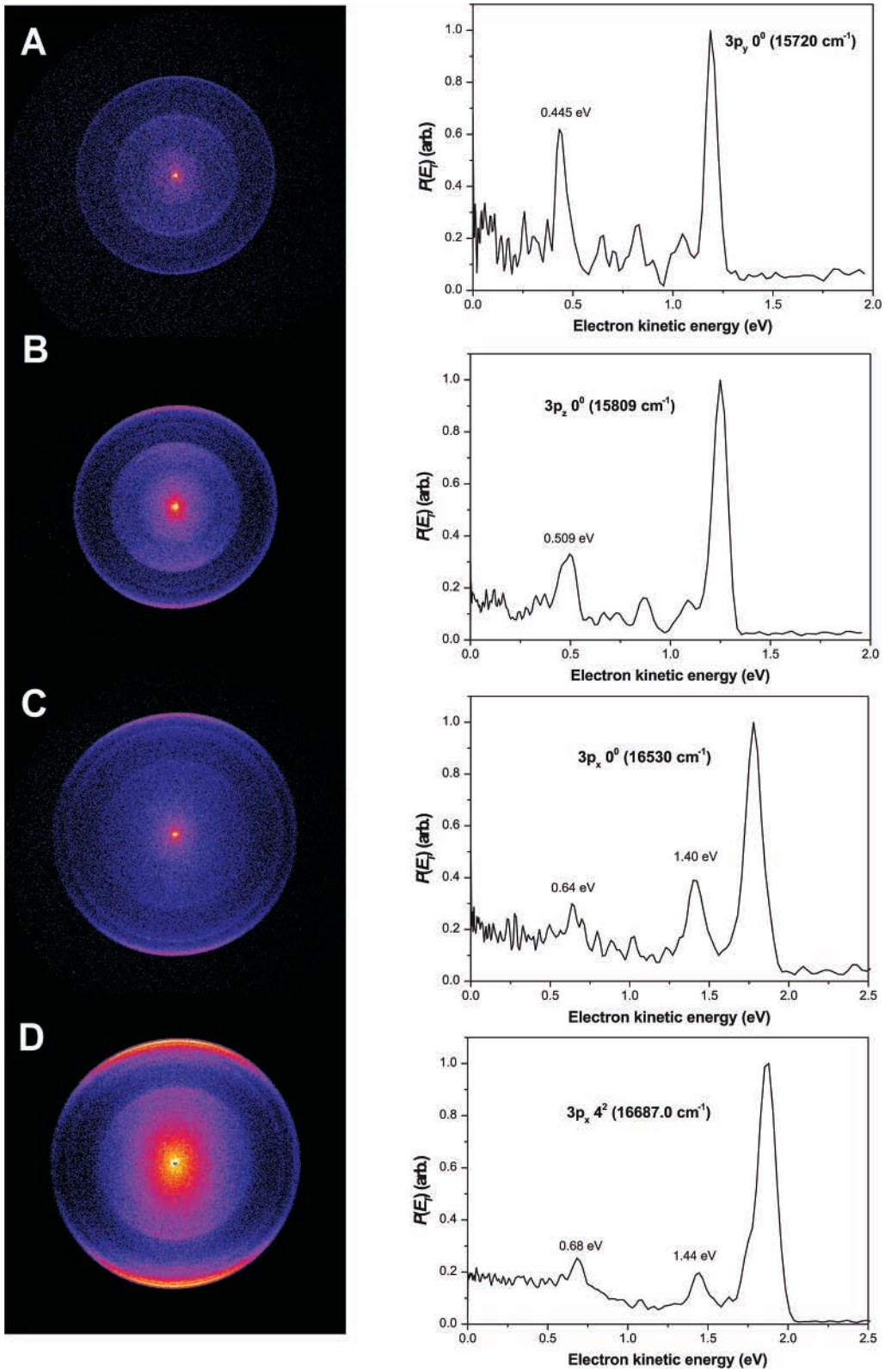

Figure 3. Photoelectron images and kinetic energy distributions measured by two-photon resonant, three-photon ionization via (π, 3p) Rydberg states at two-photon resonance energy of (A) 62 880 cm^{-1}, vibrationless excitation (υ_0); (B) 63 236 cm^{-1}, vibrationless excitation (υ_0); (C) 66 120 cm^{-1}, vibrationless excitation (υ_0); and (D) 66 748 cm^{-1}, two quanta excitation of torsional mode (υ_4), respectively. Note the slow electron kinetic energy peaks that we attribute to inter-Rydberg vibronic mixings between diagonal transitions and various origins of the lower lying Rydberg states.

immediately apparent that the three images mapped on the detector plane are spatially separated along the horizontal axis according to their mass-to-charge ratio, which clearly shows the simultaneous mass and kinetic energy multiplexing capability of the instrument. In all of these images, the rightmost image (a blurred spot) is the residual parent $C_2H_4^+$ ($m/z = 28$) ions that have virtually no recoil velocity; the next two adjacent images can be readily assigned to $C_2H_3^+$ ($m/z = 27$) and $C_2H_2^+$ ions ($m/z = 26$) that originate from the photodissociation of $C_2H_4^+$ from the indicated initial vibrational state of the ion. The

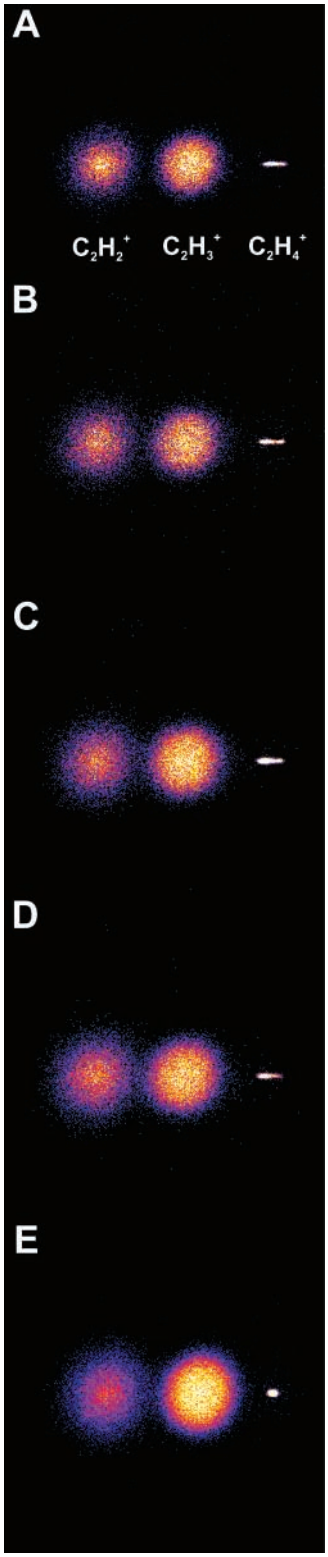

Figure 4. Experimental photofragment images from the photodissociation of $C_2H_4^+$ produced by (2 + 1) REMPI through the A: $4^3(3s)$, B: $2^14^3(3s)$, C: $0^0(3p_y)$, D: $4^2(3p_z)$, and E: $0^0(3p_x)$ vibrational states, respectively. The laser polarization was vertical in the plane of the figures.

relative intensity among the different masses in the images shows that most initially formed $C_2H_4^+$ ions undergo photofragmentation, and the two dissociation pathways, H loss and H_2 loss, are in competition, with some dependence on the initial vibrational state selection and total energy of the system. Although all photofragment images for $C_2H_3^+$ and $C_2H_2^+$ show

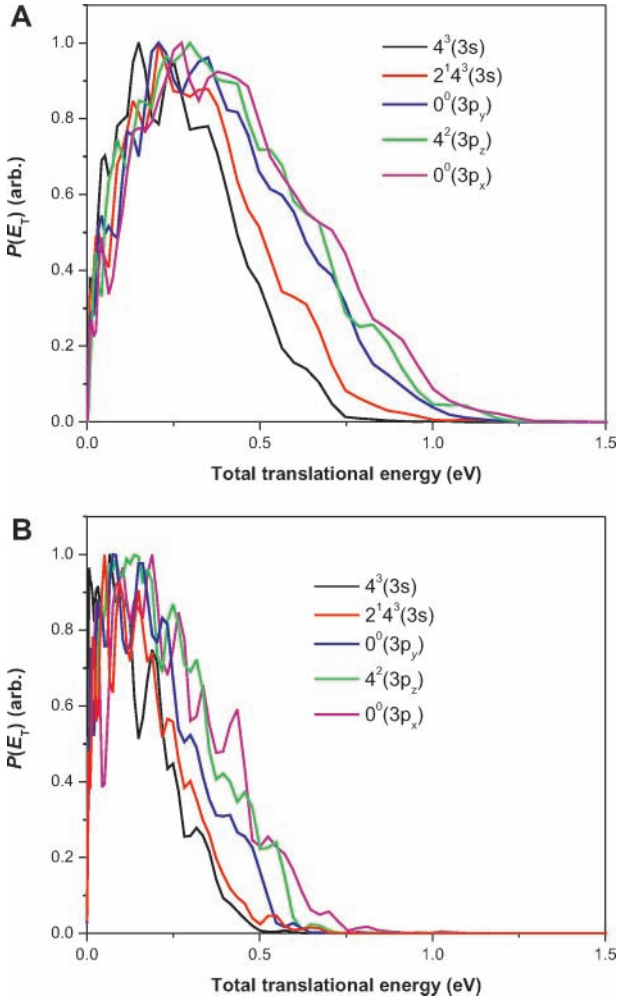

Figure 5. The total translational energy distributions for both H_2 (A) and H (B) elimination channels obtained from the images in Figure 4.

broad features and isotropic angular distributions without any distinct structure, under careful inspection a subtle difference in the shape of the images is visible between $C_2H_3^+$ and $C_2H_2^+$ dissociation channels. This difference is made clear in the translational energy distributions discussed further below.

For the higher electronically excited states of $C_2H_4^+$, the center of the $\tilde{A}^2B_{3g}$, $\tilde{B}^2A_g$, and $\tilde{C}^2B_{2u}$ ionic states are located 2.64, 4.17, and 5.61 eV, respectively, above the ground electronic state of the parent ions, 10.5127 eV (vertical IP), as determined by our own ab initio TD−DFT calculation using a B3LYP/6-311+G(d,p) basis set. These values are in good agreement with the results of high-resolution HeI PES.[36] In the photon energy range of 3.56−4.16 eV in our experimental conditions, both the $\tilde{A}^2B_{3g}$ and the $\tilde{B}^2A_g$ ionic states can be energetically accessible by one additional photon absorption of the parent cations from the ground ionic state, $\tilde{X}^2B_{3u}$. However, when considering simply symmetry selection rules for excitation under the D_{2h} point group symmetry of the ground electronic state $C_2H_4^+$ ($\tilde{X}^2B_{3u}$), only the $\tilde{B}^2A_g \leftarrow \tilde{X}^2B_{3u}$ excitation is allowed for single-photon excitation, which is consistent with the calculated nonzero transition dipole moment.

Total Translational Energy Distributions. The raw experimental data are a two-dimensional projection of the recoiling three-dimensional $C_2H_3^+$ and $C_2H_2^+$ velocity distribution. The three-dimensional distributions were reconstructed using BASEX,[34] and the total translational energy distributions, as shown in Figure 5, were obtained by integrating an appropriate slice through the three-dimensional distribution. The measured

TABLE 1: Average Total Translational Energy Values Obtained from Image Analysis for Various Vibronic Excitations of Ions

		E_{avail}(eV)		$\langle E_T \rangle$ (eV)	
excitation wavelength (λ/nm)	vibrational state of ions[a] (Rydberg state)	H	H_2	H	H_2
348.0573	4^1 (3s)	0.872	0.952	0.182	0.094
343.9263	4^3 (3s)	1.00	1.08	0.210	0.103
339.0895	2^14^1 (3s)	1.15	1.23	0.235	0.118
336.1525	2^14^3 (3s)	1.27	1.35	0.252	0.127
318.0662	0^0 ($3p_y$)	1.20	1.28	0.300	0.147
316.2755	0^0 ($3p_z$)	1.22	1.30	0.286	0.155
313.8732	4^2 ($3p_z$)	1.30	1.38	0.317	0.165
302.4803	0^0 ($3p_x$)	1.40	1.48	0.343	0.183
299.6344	4^2 ($3p_x$)	1.49	1.57	0.360	0.182
297.8407	4^4 ($3p_x$)	1.60	1.68	0.374	0.183

[a] Each vibrational state of the ions represents a predominant level obtained from REMPI-PES.

translation energy release for both H and H_2 elimination channels are relatively small with respect to total available energies in the system. As shown in Table 1, for example, the average total translational energy of H elimination channel is $\langle E_T \rangle = \sim 0.21$ eV for dissociation from the 4^3 level, while that of H_2 elimination is $\langle E_T \rangle = \sim 0.10$ eV for the same excitation. This measured average total translational energies for the 4^3 excitation accounts for only about 10% of the total available energy for the H_2 elimination and for 21% of the H elimination, respectively. One of the interesting features is that all of the translation energy distributions obtained for the H_2 elimination channel follow the typical statistical unimolecular decay pattern,[46] which represents the maximum intensity close to zero kinetic energy, whereas the maximum peaks are slightly shifted to higher kinetic energy for H elimination. In both cases, a large fraction of the available energy is partitioned into internal energy of the photofragment. Therefore, the appearances of the $P(E_T)$ and the isotropic angular distribution suggest that, for the H_2 channel, dissociation ultimately takes place on the ground electronic state following internal conversion. This is reasonably consistent with the theoretical considerations by Lorquet and co-workers.[23] As mentioned by Lorquet and co-workers,[23] however, an alternative interpretation to account for the small total translational energy for H_2 elimination can be based on energy partitioning into H_2 internal modes along the reaction path. From extensive experimental and theoretical results, the $\tilde{B}^2A_g$ excited state is believed to undergo rapid internal conversion to the vibrationally excited electronic ground state $\tilde{X}^2B_{3u}$ through the $\tilde{C}^2B_{2u}$ (which correlates to a 180° rotation about the C−C bond in the ground state molecule) or the $\tilde{A}^2B_{3g}$ state. After internal conversion, the plausible mechanism for H_2 elimination, as illustrated in Figure 1, is that the vibrationally excited $C_2H_4^+$ on the ground electronic state follows the reaction path connecting a bridged intermediate structure to ethylidene (CH_3CH^+) by hydrogen transfer. This ultimately leads to the $C_2H_2^+ + H_2$ dissociation by 1,1 elimination.[23] The relatively very low kinetic energy release, obtained for the entire range of our excitation energies, also implies that H_2 elimination from the ground electronic state of parent ions after internal conversion is most plausible.

As shown in Figure 1, for H loss, the ground state $\tilde{X}^2B_{3u}$ correlates with the first excited state of $C_2H_3^+$. On the other hand, the $\tilde{A}^2B_{3g}$ state correlates with the ground state of $C_2H_3^+$, which has the lowest asymptotic energy and $^1A'$ symmetry. A conical intersection also exists between the $\tilde{X}^2B_{3u}$ and the $\tilde{A}^2B_{3g}$ states at point C along the C−H stretching mode in Figure 1.

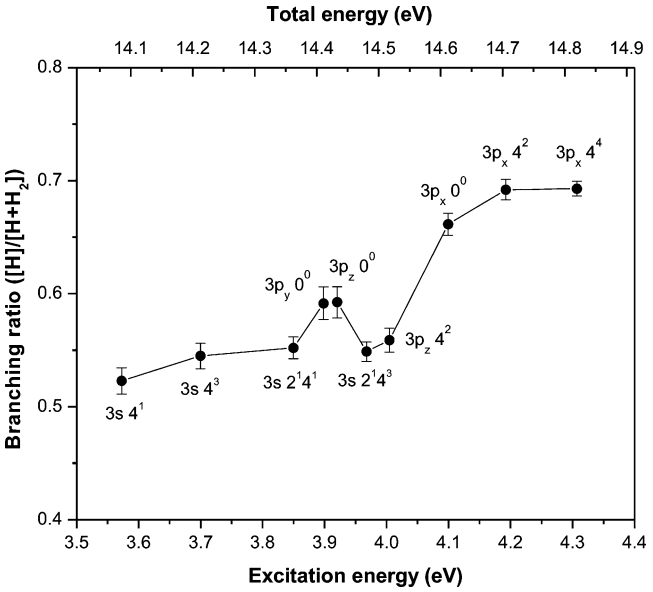

Figure 6. The branching ratio for H elimination as a function of total energy of the system from the photodissociation of $C_2H_4^+$ via the (π, 3s) and (π, 3p) Rydberg intermediate states. The excitation energy = $4h\nu$ − IP(10.5127 eV) + vibrational energy of each level. It should be noted that the 2σ error bars are estimated from the average of 10 images for each wavelength at the same condition.

After internal conversion, the vibrationally excited $C_2H_4^+$ on the ground electronic state experiences electronic coupling with the $\tilde{A}^2B_{3g}$ state around conical intersection C as one of C−H bonds is stretched. Finally, H elimination takes place along the nonadiabatic pathway to give rise to the ground state $C_2H_3^+$. Alternatively, the $\tilde{B}^2A_g$ state can undergo internal conversion to the $\tilde{A}^2B_{3g}$ state directly. For the H atom product, the peak is slightly shifted from zero. Previous studies suggested there is no evidence of an exit channel barrier correlating with the $C_2H_3^+ + H$ channel along the C−H stretching coordinate.[23] This peaking away from zero energy is commonly seen for H elimination in barrierless processes and was recently characterized in some detail by Balint-Kurti and co-workers using a statistical adiabatic product distribution (SAPD) method.[47,48] They also suggested that this substantial difference between the two different dissociation pathways can be attributed to the larger number of rotational degrees of freedom in the fragments.[47] In our case, similarly, the H_2 elimination channel can give rise to greater internal density of states than that of H elimination, which results in a higher probability for the occurrence of low relative kinetic energies.

Branching for Dissociation Pathways. By direct integration of the images, the branching ratios between H and H_2 elimination channels were also measured as a function of excitation energy, starting from different initial vibrationless or vibrationally excited levels, as shown in Figure 6. We note that the precision of these measurements, in which the 2σ error is based on the average of 10 images, reflects the strength of the multimass approach. We see from the general trend that H elimination increases with increasing total internal energy of the system. This is in complete agreement with the earlier TPEPICO results[19] and quasiequilibrium theory (QET) calculations[24] in the same energy region. However, we clearly see a reduced branching to the H elimination channel when we dissociate from the vibrationally excited parent ion as compared to those cases in which we have no initial vibrational excitation at comparable energies. We observed the same behavior in our preliminary study of *n*f Rydberg states[30] at higher total energy.

In the present study, that H_2 elimination channel is slightly enhanced with pure torsional excitation of two quanta ($3p_z\ 4^2$) or with combination excitation ($3s\ 2^1 4^3$) with υ_2 mode (C−C stretching) relative to the vibrationless excitation via the $3p_y\ 0^0$ and $3p_z\ 0^0$ levels. These results indicate that, although the two vibronic excitation wavelengths are very close to each other, the vibrational state selection of the ground electronic state of $C_2H_4^+$ ($\tilde{X}^2B_{3u}$) can have a significant effect upon the detailed dissociation dynamics. A more thorough understanding of these effects are pending further theoretical studies.

It is worth pausing to consider the difference between these experiments and the TPEPICO approach. For single-photon excitation, one accesses excited ionic states via vertical transitions from the neutral ground state geometry. In the present vibrationally mediated studies, Franck−Condon factors govern access to excited states from a range of different geometries. We might expect that any state-selective behavior would be washed out in the photodissociation of $C_2H_4^+$ following the $\tilde{B}^2A_g$ excitation, given the extensive rearrangements occurring on the ground state, so that the branching ratios would depend only on the total internal energy of the system, as in the TPEPICO case.[19] However, pure torsional excitation or combination excitation with C−C stretching vibration can have a significant effect on the Franck−Condon mediated access to various configurations of the $\tilde{B}^2A_g$ state, which may then strongly influence the relative access to the ground state or perhaps simply determine the regions of these surfaces accessed following internal conversion. It is likely because, for the ground state of ions, the torsional angle is constrained to 27°, and planar geometries are not accessed (See Figure 1B).[35] Therefore, pure torsional or combination excitation takes the system above the barrier to planarity, so that entirely different regions of the $\tilde{B}^2A_g$ state can be accessed. This situation can then influence the internal conversion rates to the $\tilde{A}^2B_{3g}$ state or the ground state or to slightly different regions of the ground state. The competition between the two different dissociation pathways is controlled by the conical intersection between the $\tilde{X}^2B_{3u}$ and the $\tilde{A}^2B_{3g}$ state along the C−H stretching mode coordinate. However, to elucidate the origin of the influence of initial vibrational state selection in the dissociation dynamics of $C_2H_4^+$, it is ultimately essential to perform dynamic calculations involving the excited state potential surfaces and nonadiabatic interaction in this challenging system.

IV. Conclusion

In summary, we report here the vibrationally mediated photodissociation dynamics of $C_2H_4^+$ through the ($\tilde{B}^2A_g$) excited state using the newly developed reflectron multimass velocity map imaging technique. Photoelectron imaging confirms the nature of the initial cation state preparation. The measured translational energy distributions and the accurate branching ratios between H and H_2 elimination provide insight into the photodissociation mechanisms and the competition between adiabatic and nonadiabatic pathways.

Acknowledgment. The authors would like to thank Professor J. C. Lorquet for his permission for use of the potential energy surfaces of $C_2H_4^+$ in ref 23. This work was supported by the National Science Foundation under award No. CHE-0415393.

References and Notes

(1) Crim, F. F. *J. Phys. Chem.* **1996**, *100*, 12725.
(2) Crim, F. F. *Acc. Chem. Res.* **1999**, *32*, 877.
(3) Hause, M. L.; Yoon, Y. H.; Crim, F. F. *J. Chem. Phys.* **2006**, *125*.
(4) Orlando, T. M.; Yang, B. R.; Anderson, S. L. *J. Chem. Phys.* **1989**, *90*, 1577.
(5) Chiu, Y. H.; Yang, B. R.; Fu, H. S.; Anderson, S. L.; Schweizer, M.; Gerlich, D. *J. Chem. Phys.* **1992**, *96*, 5781.
(6) Liu, J. B.; Van Devener, B.; Anderson, S. L. *J. Chem. Phys.* **2005**, *123*.
(7) Chandler, D. W.; Houston, P. L. *J. Chem. Phys.* **1987**, *87*, 1445.
(8) Eppink, A.; Parker, D. H. *Rev. Sci. Instrum.* **1997**, *68*, 3477.
(9) Gebhardt, C. R.; Rakitzis, T. P.; Samartzis, P. C.; Ladopoulos, V.; Kitsopoulos, T. N. *Rev. Sci. Instrum.* **2001**, *72*, 3848.
(10) Townsend, D.; Minitti, M. P.; Suits, A. G. *Rev. Sci. Instrum.* **2003**, *74*, 2530.
(11) Lin, J. J.; Zhou, J. G.; Shiu, W. C.; Liu, K. P. *Rev. Sci. Instrum.* **2003**, *74*, 2495.
(12) Vieuxmaire, O. P. J.; Nix, M. G. D.; Fitzpatrick, J. A. J.; Beckert, M.; Dixon, R. N.; Ashfold, M. N. R. *Phys. Chem. Chem. Phys.* **2004**, *6*, 543.
(13) Aguirre, F.; Pratt, S. T. *J. Chem. Phys.* **2003**, *118*, 6318.
(14) Nahler, N. H.; Vieuxmaire, O. P. J.; Jones, J. R.; Ashfold, M. N. R.; Eppink, A.; Coriou, A. M.; Parker, D. H. *J. Phys. Chem. A* **2004**, *108*, 8077.
(15) Webb, A. D.; Nahler, N. H.; Dixon, R. N.; Ashfold, M. N. R. *J. Chem. Phys.* **2006**, *125*.
(16) Chang, C. S.; Luo, C. Y.; Liu, K. *J. Phys. Chem. A* **2005**, *109*, 1022.
(17) Kim, M. H.; Shen, L.; Suits, A. G. *Phys. Chem. Chem. Phys.* **2006**, *8*, 2933.
(18) Kim, M. H.; Shen, L.; Tao, H. L.; Martinez, T. J.; Suits, A. G. *Science* **2007**, *315*, 1561.
(19) Stockbauer, R.; Inghram, M. G. *J. Chem. Phys.* **1975**, *62*, 4862.
(20) Mackie, R. A.; Scully, S. W. J.; Sands, A. M.; Browning, R.; Dunn, K. F.; Latimer, C. J. *Int. J. Mass Spectrom.* **2003**, *223*, 67.
(21) Pollard, J. E.; Trevor, D. J.; Reutt, J. E.; Lee, Y. T.; Shirley, D. A. *J. Chem. Phys.* **1984**, *81*, 5302.
(22) Malow, M.; Guthe, F.; Weitzel, K. M. *Phys. Chem. Chem. Phys.* **1999**, *1*, 1425.
(23) Sannen, C.; Raseev, G.; Galloy, C.; Fauville, G.; Lorquet, J. C. *J. Chem. Phys.* **1981**, *74*, 2402.
(24) Desouterlecomte, M.; Sannen, C.; Lorquet, J. C. *J. Chem. Phys.* **1983**, *79*, 894.
(25) Oblinger, M.; Lorquet, A. J.; Lorquet, J. C. *Int. J. Mass Spectrom.* **1997**, *167*, 149.
(26) Costa, F. *Int. J. Quantum Chem.* **2006**, *106*, 2763.
(27) Tsai, S. T.; Lin, C. K.; Lee, Y. T.; Ni, C. K. *Rev. Sci. Instrum.* **2001**, *72*, 1963.
(28) Leskiw, B. D.; Kim, M. H.; Hall, G. E.; Suits, A. G. *Rev. Sci. Instrum.* **2005**, *76*.
(29) Kim, M. H.; Leskiw, B. D.; Shen, L.; Suits, A. G. *Int. J. Mass Spectrom.* **2006**, *252*, 73.
(30) Kim, M. H.; Leskiw, B. D.; Suits, A. G. *J. Phys. Chem. A* **2005**, *109*, 7839.
(31) Williams, B. A.; Cool, T. A. *J. Chem. Phys.* **1991**, *94*, 6358.
(32) Rijkenberg, R. A.; Buma, W. J. *J. Phys. Chem. A* **2002**, *106*, 3727.
(33) Li, W.; Chambreau, S. D.; Lahankar, S. A.; Suits, A. G. *Rev. Sci. Instrum.* **2005**, *76*.
(34) Dribinski, V.; Ossadtchi, A.; Mandelshtam, V. A.; Reisler, H. *Rev. Sci. Instrum.* **2002**, *73*, 2634.
(35) Willitsch, S.; Hollenstein, U.; Merkt, F. *J. Chem. Phys.* **2004**, *120*, 1761.
(36) Holland, D. M. P.; Shaw, D. A.; Hayes, M. A.; Shpinkova, L. G.; Rennie, E. E.; Karlsson, L.; Baltzer, P.; Wannberg, B. *Chem. Phys.* **1997**, *219*, 91.
(37) Xing, X.; Bahng, M. K.; Wang, P.; Lau, K. C.; Baek, S. J.; Ng, C. Y. *J. Chem. Phys.* **2006**, *125*.
(38) Patsilinakou, E.; Wiedmann, R. T.; Fotakis, C.; Grant, E. R. *J. Chem. Phys.* **1989**, *91*, 3916.
(39) Wiedmann, R. T.; Grant, E. R.; Tonkyn, R. G.; White, M. G. *J. Chem. Phys.* **1991**, *95*, 746.
(40) Morgan, R. A.; Puyuelo, P.; Howe, J. D.; Ashfold, M. N. R.; Buma, W. J.; Milan, J. B.; Delange, C. A. *J. Chem. Soc., Faraday Trans.* **1994**, *90*, 3591.
(41) Morgan, R. A.; Puyuelo, P.; Howe, J. D.; Ashfold, M. N. R.; Buma, W. J.; Wales, N. P. L.; Delange, C. A. *J. Chem. Soc., Faraday Trans.* **1995**, *91*, 2715.
(42) Morgan, R. A.; Orrewing, A. J.; Ashfold, M. N. R.; Buma, W. J.; Wales, N. P. L.; Delange, C. A. *J. Chem. Soc., Faraday Trans.* **1995**, *91*, 3339.
(43) Dobber, M. R.; Buma, W. J.; Delange, C. A. *J. Chem. Phys.* **1993**, *99*, 836.
(44) Hillenbrand, S.; Zhu, L. C.; Johnson, P. *J. Chem. Phys.* **1990**, *92*, 870.
(45) Wright; McKoy; Stolow; Jortner; Muller-Dethlefs; Texier; Vrakking; Fischer; Baer; Child; Ashfold; de Lange; Donovan; Reid; Powis;

Davies; Dyke; Johnson; Neumark; Thomas, J. M.; Continetti; Hepburn; Schlag; Softley; Fielding; Hiyama; Reinhold, *Faraday Discuss.* **2000**, *115*, 79.

(46) Klots, C. E. *J. Chem. Phys.* **1976**, *64*, 4269.

(47) Cole, J. P.; Balint-Kurti, G. G. *J. Chem. Phys.* **2003**, *119*, 6003.

(48) Feltham, E. J.; Qadiri, R. H.; Cottrill, E. E. H.; Cook, P. A.; Cole, J. P.; Balint-Kurti, G. G.; Ashfold, M. N. R. *J. Chem. Phys.* **2003**, *119*, 6017.